*Chinese Journal of*
**POLYMER SCIENCE**

RESEARCH ARTICLE

https://doi.org/10.1007/s10118-024-3096-6
*Chinese J. Polym. Sci.*

# Polyelectrolyte Complexes and Coacervates Formed by *De novo*-Designed Peptides and Oligonucleotide

Tian-Hao Ren and De-Hai Liang*

*Beijing National Laboratory for Molecular Sciences, Department of Polymer Science and Engineering and the Key Laboratory of Polymer Chemistry and Physics of the Ministry of Education, College of Chemistry and Molecular Engineering, Peking University, Beijing 100871, China*

Electronic Supplementary Information

**Abstract** The liquid-liquid phase separation of biopolymers in living cells contains multiple interactions and occurs in a dynamic environment. Resolving the regulation mechanism is still a challenge. In this work, we designed a series of peptides $(XXLY)_6SSSGSS$ and studied their complexation and coacervation behavior with single-stranded oligonucleotides. The "X" and "Y" are varied to combine known amounts of charged and non-charged amino acids, together with the introduction of secondary structures and pH responsiveness. Results show that the electrostatic interaction, which is described as charge density, controls both the strength of complexation and the degree of chain relaxation, and thus determines the growth and size of the coacervates. The hydrophobic interaction is prominent when the charges are neutralized. Interestingly, the secondary structures of peptides exhibit profound effect on the morphology of the phases, such as solid phase to liquid phase transition. Our study gains insight into the phase separation under physiological conditions. It is also helpful to create coacervates with desirable structures and functions.

**Keywords** Polyelectrolyte complex; Coacervate; Peptides; Secondary structure; Electrostatic interaction

**Citation:** Ren, T. H.; Liang, D. H. Polyelectrolyte complexes and coacervates formed by *De novo*-designed peptides and oligonucleotide. *Chinese J. Polym. Sci.* https://doi.org/10.1007/s10118-024-3096-6

## INTRODUCTION

Polyelectrolyte complexes, which are formed by oppositely charged polyelectrolytes, can further undergo phase separation to form solid precipitates, liquid coacervates, or gels.[1–5] Because the liquid coacervates share the same mechanism as membraneless organelles, such as stress granules, Cajal bodies, and nucleoli, it has attracted a great deal of attention in recent years.[6–9] Coacervates have found applications in protein encapsulation,[10,11] drug delivery to cells,[12–15] personal care products,[16,17] underwater adhesives,[18,19] and so on.[20] Moreover, coacervates have been proposed as protocell models to explore the origin of life on early Earth about one hundred years ago.[21–24]

Electrostatic interaction is generally believed to play a key role during the complexation and coacervation processes.[25] The release of counter ions, which causes a strong entropic gain, is the main driving force for polyelectrolyte complexes.[26] The theories on coacervation, such as Voorn-Overbeek theory,[27,28] Polymer field theory,[29,30] and Scaling theory,[31,32] treat electrostatic attraction as the leading contribution, which involves both salt concentration and counterion releases.[33] For the coacervates formed by biopolymers, especially proteins and peptides, the non-electrostatic interactions such as hydrophobic interaction could play an essential role in the phase separation process.[34,35] The chain rigidity and the secondary structures, which are related to the sequence of amino acids, are not negligible either.[36–38] Moreover, the cellular interior is a heterogeneous and dynamic environment. The variations in salt concentration and pH value could also regulate the coacervation process.[39–43] The electrostatic and non-electrostatic interactions, as well as the environmental effects, are correlated together. Resolving these effects and their regulation on the coacervation under dynamic conditions is still a challenge.[26]

*De novo* design of peptides with proper sequence offers a practical approach to combine the known amount of charged and non-charged amino acids together, which could also introduce desirable secondary structures and pH responsiveness.[44–46] A comparison of the complexes or coacervates formed by such peptides should be able to reveal the cooperation mechanism of these effects. In this work, we designed 7 peptides with the sequence of $(XXLY)_6SSSGSS$ (Table 1). Here, X in the repetitive segment stands for the positively charged Arginine (R) or Histidine (H), while Y stands for R, H, negatively charged Glutamate (E), or polar Cysteine (C). Leucine (L) is to introduce hydrophobic interaction in the complex, while the hydrophilic segment SSSGSS is to reduce the surface ten-

* Corresponding author, E-mail: dliang@pku.edu.cn

Special Issue: Charged Polymers
Received November 27, 2023; Accepted January 12, 2024; Published online March 4, 2024

**Table 1** Physicochemical parameters of the designed peptides.

| Peptides | Molecular weight | p*I* | GRAVY | Net charge | | |
|---|---|---|---|---|---|---|
| | | | | pH 8.0 | pH 6.0 | pH 4.0 |
| RRLR | 4000 | 13.6 | −2.09 | 18 | 18 | 18 |
| RRLC | 3682 | 12.2 | −0.69 | 10 | 12 | 12 |
| RRLE | 3838 | 12.2 | −1.89 | 6 | 6 | 10 |
| HHLR | 3772 | 13.1 | −1.57 | 6 | 12 | 18 |
| HHLH | 3658 | 8.48 | −1.31 | 0 | 9 | 18 |
| HHLC | 3454 | 7.33 | −0.17 | −2 | 6 | 12 |
| HHLE | 3610 | 6.02 | −1.37 | −6 | 0 | 10 |

sion of the complex or coacervate.[47] These peptides are named the repetitive segment XXLY. RRLR is proven to be able to form coacervates with ss-oligo as demonstrated in our former work.[47] The calculated physicochemical parameters of these peptides, including isoelectric point (p*I*), grand average of hydropathy (GRAVY),[48] and effective charges at varying pH values, are also listed in Table 1. The calculation program is based on Stothrad's method.[49] The p$K_a$ values of amino acids are given by Lehninger *et al*.[50] The p*I* values range from 6.02 (HHLE) to 13.6 (RRLR). Therefore, RRLR is independent of pH from 4.0 to 8.0, while HHLE carries opposite charges at pH 4.0 and pH 8.0. Note that the hydrophobicity as indicated by the GRAVY value is the sum of the hydropathy values of all the amino acids, with RRLR being the least hydrophobic peptide and HHLC being the most hydrophobic peptide. Actually, the hydrophobicity of the backbone (charge is neutralized) accounts for the contribution to the complexation or coacervation process. 21-nt Single-stranded oligonucleotide (ss-oligo) is used to form complexes with the peptides at a +/− charge ratio close to unity. Results show that both the charge density and hydrophobic interaction are responsible for the complexes and coacervates formed by peptides and ss-oligo. Interestingly, the secondary structure, which is pH-dependent, exhibits an effect even stronger than the electrostatic interactions.

## EXPERIMENTAL

### Materials

The 21-nt ss-oligo samples of arbitrary sequence (CTTACGCTGAGTACTTCGATT) with and without cy5 labeling at 5′ end were purchased from Invitrogen Inc (Shanghai, China). The purity is >99% and no further purification was conducted. The ss-oligo sample was dissolved in deionized water to obtain a stock solution of 6.0 mg/mL, then added with a 1.0% weight fraction of cy5-labeled ss-oligo to track the distribution. The peptides with a purity >95% were purchased from Scilight Peptide (Beijing, China) and were also used without further purification. The peptides were dissolved in deionized water to prepare the stock solutions with the concentration ranging from 3.7 mg/mL for HHLH to 7.0 mg/mL for RRLE depending on the charge density and molecular weight so that the +/− charge ratio was 1.0 when the peptide and ss-oligo were mixed with equal volume at pH 4.0. Polyvinylpyrrolidone (PVP, $M_w$ ~30000) was purchased from Sinopharm Chemical Reagon (Beijing, China) and used as received.

### Coacervation Monitored by Confocal Microscope

The coacervates were prepared in a circular well with 3.0 mm in diameter and 2.0 mm in depth. A cover glass is glued on the bottom of the well to facilitate the observation by microscopy. The sample well was washed in sequence with water, 1.0 mol/L NaOH, water, 1.0 mol/L HCl, and water, each for 2.0 min. 1.0% PVP was then applied to dynamically coat the glass to inhibit molecular adsorption. For a better comparison of the pH effect on coacervation, the peptides and the ss-oligo stock solutions were diluted for 4 times by the same 20 mmol/L PBS buffers but tuned to pH 8.0, pH 6.0, or pH 4.0, separately. NaCl (200 mmol/L) was added to the buffer beforehand to alleviate the effect of ionic strength. The final concentrations are as follows: ss-oligo, 1.5 mg/mL, RRLR, 1.0 mg/mL, RRLC, 1.4 mg/mL, RRLE, 1.8 mg/mL, HHLR, 1.0 mg/mL, HHLH, 1.0 mg/mL, HHLC, 1.3 mg/mL, and HHLE, 1.7 mg/mL. 6.0 μL of peptide and 6.0 μL of ss-oligo were mixed in a 500 μL of polyethylene centrifuge tube. The moment of mixing was set as time zero. 10 μL of mixture was immediately added to the sample well, and the coacervation process was monitored on-line by Laser Scanning Confocal Microscope (A1R-si, Nikon. Co. Ltd, Japan). The excitation ($\lambda_{ex}$) and emission wavelength ($\lambda_{em}$) for Cy5 were 628 and 700 nm, respectively. The morphologies of the coacervates in the first 30 min were recorded, and the "analyze particle" function in ImageJ software was used for quantitative analysis of the images.

### Circular Dichroism (CD)

CD spectra of the peptides before and after forming complexes with ss-oligo were recorded at room temperature using MOS-500 spectropolarimeter (Bio-Logic, France). To alleviate the interference of chloride ions, 20 mmol/L PBS containing 20 mmol/L NaCl was used to dilute the samples. The final concentration of ss-oligo was 0.15 mg/mL, while the peptides were diluted accordingly to obtain the complex at +/−=1.0 after mixing with equal volumes. The ss-oligo/peptides complexes were incubated for 10 min and then loaded in a 0.1 cm path length quartz cuvette for CD measurement. The beta structure selection method (BeStSel) software was used to determine the content of the secondary structures from the CD spectra.

### Laser Light Scattering (LLS)

The complexation process of peptides and ss-oligo was monitored by a commercialized laser light scattering setup (Brookhaven Instrument Corporation, BI-200SM Goniometer, Holtsville, NY). A vertically polarized, 17 mW He-Ne laser (Newport, USA) operating at 633 nm was used as the light source. The scattered angle was fixed at 90° to ensure an uninterrupted measurement of the whole process. The excess absolute time-averaged scattered intensity was recorded to compare the degree of complexation. In dynamic light scattering (DLS), the intensity-intensity time correlation function $G^{(2)}(\tau)$ in the self-beat-

https://doi.org/10.1007/s10118-024-3096-6

ing mode was measured. A Laplace inversion program, CONTIN, was applied to obtain the line width distribution and the diffusion coefficient $D$. The diffusion coefficient can be further converted into the hydrodynamic radius $R_h$ by using the Stokes-Einstein equation:

$$D = k_B T / 6\pi\eta R_h \quad (1)$$

where $k_B$, $T$, $\eta$ are the Boltzmann constant, the absolute temperature, and the viscosity of the solvent, respectively.

A sample vial for LLS was dust-freed beforehand. The peptide solution in 20 mmol/L PBS (pH 8, 200 mmol/L NaCl) was filtered into the vial through a 0.22 μm syringe filter (Sartorius Stedim Minisart®, Germany). A known amount of ss-oligo solution in the same buffer but at a concentration three orders higher was filtered into the solution to avoid the dilution effect. The final concentration of ss-oligo was 0.015 mg/mL, and the +/− charge ratio was 1.0 at pH 4.0. The moment of mixing was set as time zero. The mixture was briefly vortexed and immediately measured by LLS. As the complex solution was stabilized, a known amount of 1.2 mol/L HCl was filtered into the vial to tune the pH value to 4.0. LLS measurement was taken by following the same procedure.

## RESULTS AND DISCUSSION

### Coacervation at Different pH values

Fig. 1 compares the morphologies of the phases formed by peptides and ss-oligo in aqueous solution at different pH values. All the other conditions are kept constant. Liquid coacervates are formed in most of the cases at pH 4.0 (Fig. 1c), while a variety of morphologies, including liquid coacervates, gels, and solid precipitates are observed at pH 8.0 (Fig. 1a). The degree of phase separation at pH 6.0 (Fig. 1b) is in between, but there are exceptions. Based on the pH-dependent phase separation behavior, the peptides are divided into three categories.

#### *Cat1. RRLR and HHLR*

Liquid coacervates are formed under all the studied conditions (Movie S1 in the electronic supplementary information, ESI). The growth of the coacervates is mainly by Brownian motion coalescence[51] (Fig. S1 in ESI). The liquid-liquid phase separation process can be satisfactorily explained purely by electrostatic interactions. RRLR is fully charged under all the studied pH values. Therefore, the liquid phase separation processes are very similar and exhibit no prominent pH dependence, as demonstrated by the average size of the droplets (Fig. 2). The effective charges of HHLR are sharply reduced from 18 at pH 4.0 to 6 at pH 8.0. The liquid-liquid phase separation process is thus deteriorated with increasing pH, as demonstrated by the reduced size of the droplets. Such phenomena could be attributed to the reduced +/− ratio at elevated pH values. Interestingly, the size of the droplets at pH 6.0 is larger than that at pH 4.0 (Fig. 2), even though the effective charges of HHLR reduce to 9. We attribute it to the fast relaxation of polyelectrolyte chains caused by lower charge densities. The droplets are therefore prone to grow larger at pH 6.0.

#### *Cat2. HHLH, HHLC and HHLE*

Both electrostatic interaction and hydrophobic interaction account for the phase separation process. HHLH and HHLC are neutral or close to neutral at pH 8.0, while HHLE is negatively charged at pH 8.0 and close to neutral at pH 6.0. Therefore, no coacervates are formed under such conditions. The former two

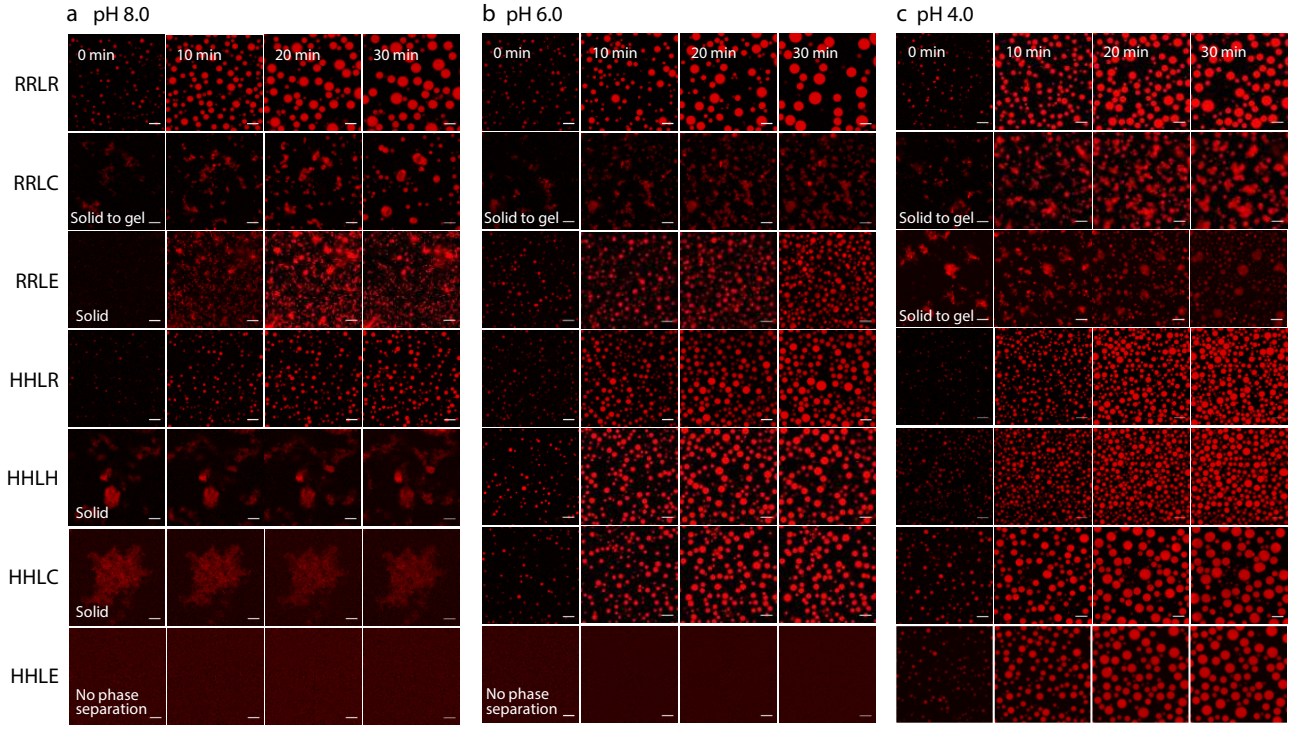


**Fig. 1** Time series of snapshots showing the morphologies of the phases formed by peptide and ss-oligo at (a) pH 8.0, (b) pH 6.0, and (c) pH 4.0. The final concentration of ss-oligo is 1.5 mg/mL, and Cy5-labeled ss-oligo is applied to show the fluorescence (red color). Scale bar: 10 μm. The "solid", "solid to gel", and "no phase separation" are marked on the corresponding panels, except those forming only coacervates.

https://doi.org/10.1007/s10118-024-3096-6

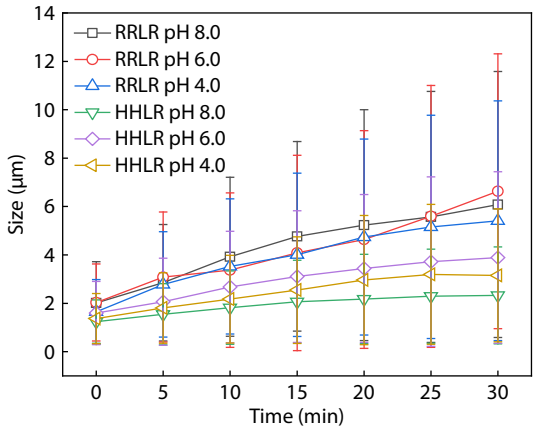


**Fig. 2** Average sizes of the coacervates formed by RRLR and HHLR with ss-oligo at varying pH values.

peptides are not soluble at pH close to p*I*. They form precipitates by themselves because the hydrophobic interaction is dominant when charges are neutralized. HHLE is soluble in water even at pH 6.0 due to the highly charged glutamate group.

At pH 4.0, all three peptides are positively charged, and they form liquid coacervates with ss-oligo. Even though the charge of HHLH is the highest, its coacervation rate is lower and the droplet size is smaller than those of the coacervates formed by HHLC and HHLE (Fig. 3), which could also be attributed to the fast relaxation caused by lower charge density. HHLH and HHLE also form liquid coacervates with ss-oligo at pH 6.0.

The coacervate size of ss-oligo/HHLH at pH 6.0 is larger than that at pH 4.0, while the ss-oligo/HHLC coacervate shows an opposite trend (Fig. 3). The reduced charge density generates dual effects: facilitating chain relaxation and deteriorating complexation. The effective charge for HHLH is 9, while the number is 6 for HHLE at pH 6.0. The charge density of HHLH is strong enough to maintain a coacervation with faster chain relaxation, while weak complexation is the dominant effect because the charge density of HHLE is too low.

### *Cat3. RRLC and RRLE*

The p*I* values of RRLC and RRLE are identical. However, they exhibit different phase separation processes with ss-oligo (Fig. 1), which cannot be explained by either electrostatic interaction or hydrophobic interaction. RRLC forms solid precipitates with ss-oligo at the early stage at all the studied pH values. The growth is *via* cluster-cluster connection at pH 8.0 (Movie S2 in ESI), pH 6.0 (Movie S3 in ESI), and pH 4.0 (Movie S4 in ESI). As the size reaches certain values, the solid precipitates transform into a gel or liquid-like state, especially at pH 4.0, as demonstrated by the spherical-like or smooth surfaces. RRLE forms solid precipitates with ss-oligo in the studied period at pH 8.0 (Movie S5 in ESI), while it forms liquid coacervates with ss-oligo throughout the experiments at pH 6.0 (Movie S6 in ESI). At pH 4.0, solid precipitates are formed at the beginning. But almost all the precipitates transform into liquid coacervate at the ending stage (Movie S7 in ESI).

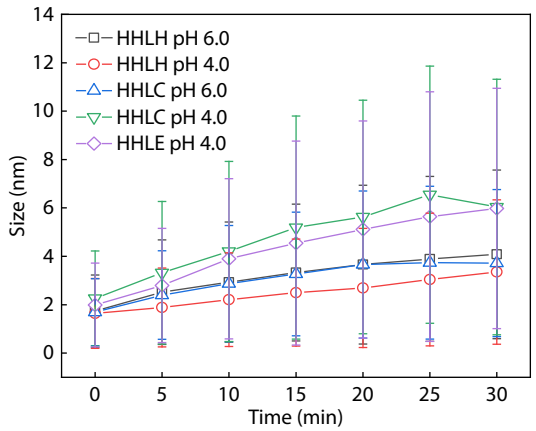


**Fig. 3** Average sizes of the coacervates formed by HHLH, HHLC, and HHLE. All these coacervates are spherical and distributed uniformly.

The solid-to-liquid phase transition could be related to the secondary structures of the peptides. To test this hypothesis, we conducted CD measurements on RRLC and RRLE before and after the formation of complexes with ss-oligo at varying pH values. Fig. 4 compares the CD curves, and the fitting results are listed in Table 2. The secondary structures are pH-dependent. RRLC forms more $\alpha$-helix and less $\beta$-sheet with decreasing pH. The $\alpha$-helix content jumps from 3.8% to 18.5%, while the $\beta$-sheet content drops from 28.4% to 16.3% as the pH value decreases from 8.0 to 4.0. RRLE exhibits the opposite trend. Its $\beta$-sheet content is much higher than that of $\alpha$-helix, the latter is negligible and reaches zero at pH 4.0.

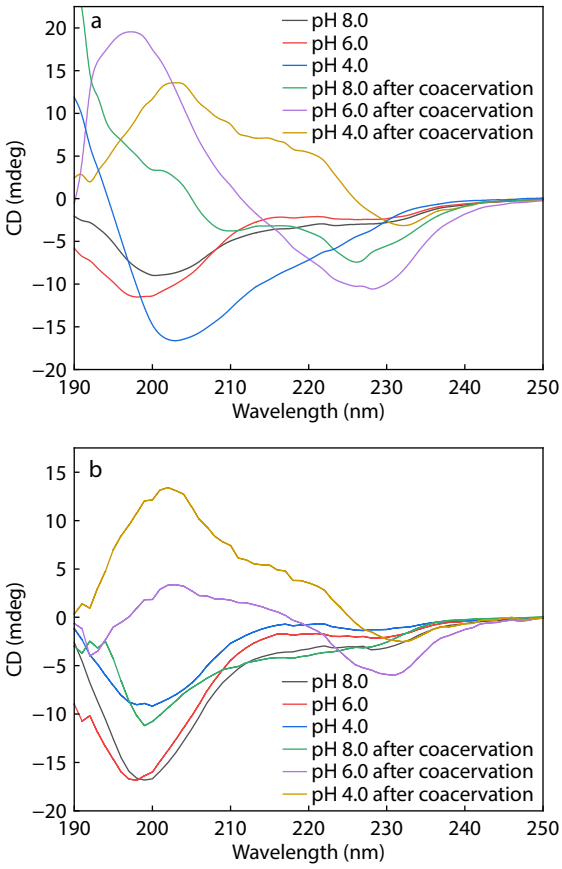


**Fig. 4** Circular dichroism spectra of (a) RRLC and (b) RRLE before and after forming complexes with ss-oligo.

https://doi.org/10.1007/s10118-024-3096-6

**Table 2** Secondary structures of RRLC and RRLE.

| Peptides | pH | $\alpha$-Helix | $\beta$-Sheet | $\beta$-Turn | Random |
|---|---|---|---|---|---|
| RRLC | 8.0 | 3.8 | 28.4 | 16.5 | 51.2 |
| | 6.0 | 1.3 | 29.4 | 17.9 | 51.5 |
| | 4.0 | 18.5 | 16.3 | 17.3 | 47.8 |
| RRLC/ss-oligo | 8.0 | 19.5 | 22.6 | 19.0 | 38.9 |
| | 6.0 | 3.7 | 44.6 | 16.9 | 44.8 |
| | 4.0 | 0 | 35.7 | 24.3 | 40.0 |
| RRLE | 8.0 | 1.3 | 26.7 | 18.3 | 49.0 |
| | 6.0 | 0.4 | 30.4 | 19.8 | 49.4 |
| | 4.0 | 0 | 31.4 | 17.9 | 50.8 |
| RRLE/ss-oligo | 8.0 | 6.6 | 32.3 | 19.2 | 41.9 |
| | 6.0 | 4.3 | 24.4 | 26.3 | 45.0 |
| | 4.0 | 0 | 37.7 | 23.8 | 38.5 |

Because $\beta$-sheet is formed by inter-chain hydrogen bonds, the negatively charged glutamate in RRLE facilitates the formation of $\beta$-sheet.

Upon forming complexes with ss-oligo, the secondary structures of the peptides are different due to charge neutralization and local enhanced concentration. At pH 8.0, an increase in $\alpha$-helix occurs, especially for RRLC, whose $\alpha$-helix content reaches 19.5%. At pH 4.0, the $\beta$-sheet content of both peptides increases prominently. Because $\alpha$-helix and $\beta$-sheet introduce ordered structures into the complex, solid precipitates are the preferred morphology. The corresponding decrease in random structure, which accounts for the liquid coacervates, also confirms this conclusion.

The case at pH 6.0 is special. As for RRLC, both the $\beta$-sheet and the random structure increase their contents in the complex. The effect of high $\beta$-sheet content (44.6%) is dominant, generating solid precipitates that are difficult to transform into gels or liquid coacervates (Movie S3 in ESI). Interestingly, the $\beta$-sheet content of RRLE is extremely low in the complex, only 24.4% at pH 6.0, while the random structure maintains its highest content (45%). Both facilitate the formation of liquid coacervates (Movie S6 in ESI). Currently, we do not have explanations for the formation of the abnormal amount of specific secondary structures in the complex at pH 6.0.

## Complexation Studied by LLS

To further reveal the interactions governing the phase separation process, we conducted LLS measurements to on-line monitor the complexation of peptides with ss-oligo. More importantly, LLS is able to monitor the kinetic process as the pH jumps from 8.0 to 4.0. Because the sizes of the coacervates in Fig. 1 are beyond the scope of LLS, the concentrations of ss-oligo and peptides are lowered by three orders to reduce the sizes. At pH 8.0, RRLE and HHLE do not form complexes with ss-oligo, while HHLH and HHLC form precipitates (cloudy) with ss-oligo under the studied conditions.

The whole complexation of RRLR, RRLC, or HHLR with ss-oligo can be monitored, but their behaviors are quite different. As shown in Fig. 5, only the mode corresponding to the complex is observed by DLS. Because the concentrations of the complexes are close, and the refractive index increments of peptides and ss-oligo are similar, the excess scattered intensity indicates the changes in the molecular weight of the complexes. The intensity of the ss-oligo/RRLR complex decreases with time (Fig. 5d), while the hydrodynamic radius shows an opposite trend (Fig. 5e). These results suggest that the initially formed complex undergoes a relaxation and swelling process, which is reasonable because the concentrated ss-oligo results in a complex with higher density but smaller size upon mixing with RRLR. The scattered intensity of the ss-oligo/RRLC complex increases at the beginning and starts to decline after reaching a peak value, while the size monotonously increases with time. We attribute such behavior to the cysteine group, which reduces the charge density of the peptide and the hydrophobicity of the formed complex, leading to slow complexation and swelling processes. Both the scattered intensity and the size of ss-oligo/HHLR exhibit weak time dependence. The complex is stable in the studied period.

As the pH value is dropped from 8.0 to 4.0, all the peptides form complexes with ss-oligo, and the whole process is monitored by LLS (Fig. 6). Again, only the complexes are observed in DLS (Fig. S2 in ESI). Based on the excess scattered intensity and the sizes of the complexes, the peptides can be divided into two categories, which are different from the results based on phase separation behavior (Fig. 1).

RRLR, RRLC, HHLR and HHLH interact strongly with ss-oligo, forming complexes with scattered intensities several times higher than those formed by the rest of the peptides (Fig. 6a). The sizes of the complexes are also significantly larger (Fig. 6b). The intensity of the complexes decreases with time while the size exhibits an opposite trend, suggesting that the initially formed complexes undergo a relaxation and swelling process. The effective charges of RRLR, HHLR, and HHLH are equal and reach the maximum value of 18 after the pH jump, which accounts for the heavy complexation processes. The effective charges of RRLC are only 12. However, the complex formed by RRLC and ss-oligo exhibits the highest scattered intensity (Fig. 6a), which is not normal. Because RRLC and HHLR already form complexes with ss-oligo at pH 8.0 (Fig. 5), the enhancement in charge density results in a secondary complexation process, which is demonstrated as an increase in the excess scattered intensity in the beginning, followed by the relaxation afterward (Fig. 6a). The charge density of RRLR does not change after a pH jump. We attribute the adjustment to the disturbance of local pH and enhanced ionic strength induced by the addition of 1.2 mol/L HCl, which results in slightly lower intensity and larger size compared with those values at pH 8.

RRLE, HHLE, and HHLC form complexes with ss-oligo but

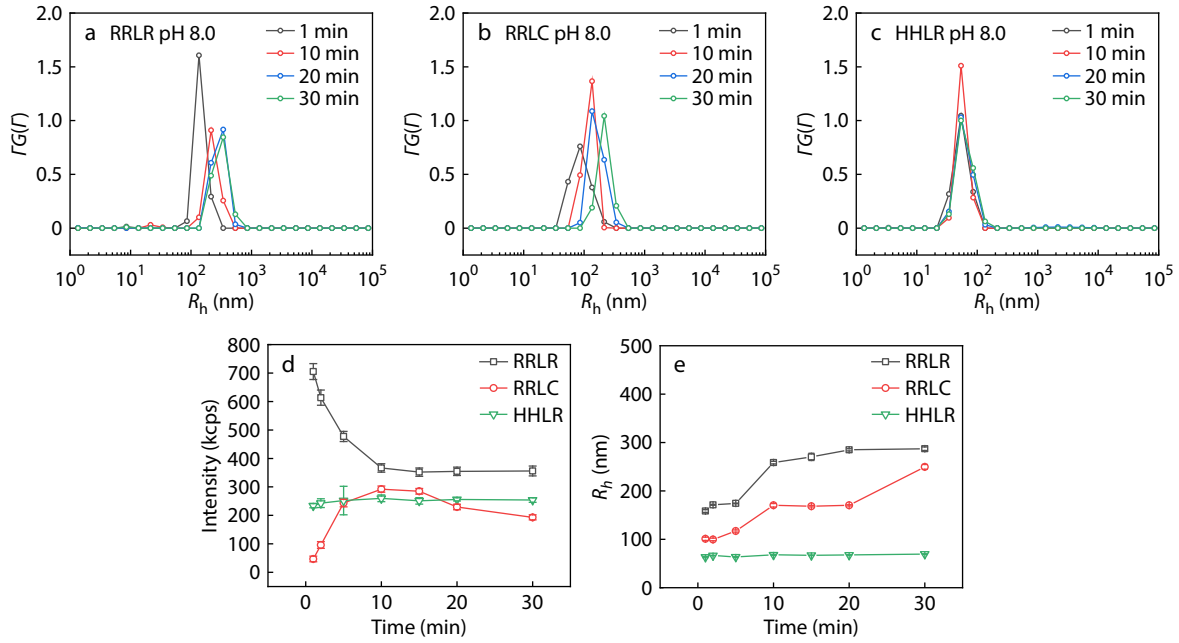


**Fig. 5** Light scattering study on the peptide/ss-oligo complexes at pH 8.0. Size distribution of the complex formed by ss-oligo with (a) RRLR, (b) RRLC, and (c) HHLR. (d and e) Compare the excess scattered intensity and the average hydrodynamic radius of the complexes, respectively. Scattering angle: 90°.

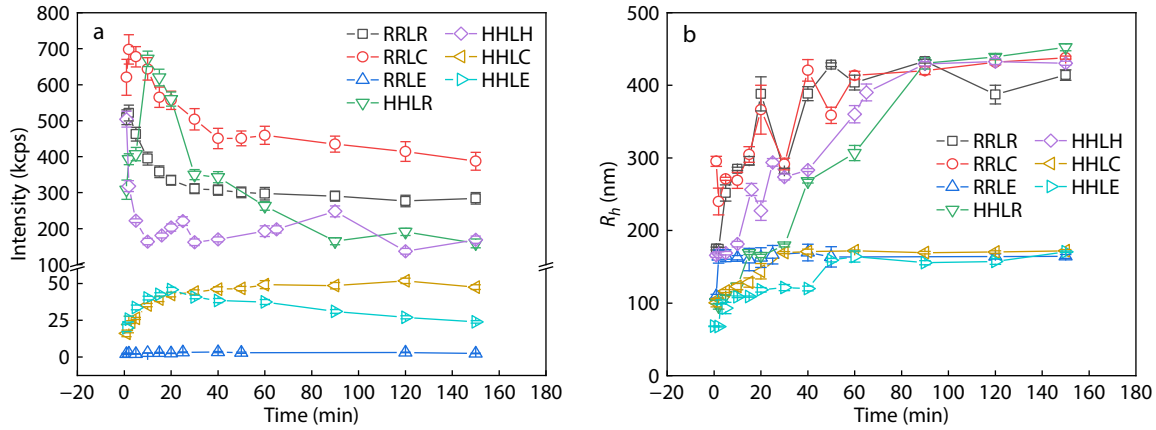


**Fig. 6** Time dependence of the excess scattered intensity (a) and the hydrodynamic radius (b) of the complexes formed by ss-oligo with peptides as the pH jumps from 8.0 to 4.0. Scattering angle: 90°.

with much lower intensity and hydrodynamic radius, which could be attributed to the lower effective charges (10 or 12). The charge densities of RRLE and HHLE are very similar. However, the former forms a complex with a comparable size but much lower scattered intensity. No relaxation process is observed either. HHLC possesses the same charge density as RRLC. However, the complex formed by RRLC shows a much higher scattered intensity and size. The abnormal complex behaviors of RRLE and RRLC as determined by LLS agree with the findings on phase separation by microscopy (Fig. 1), which could be explained by the formation of secondary structures upon forming complexes with ss-oligo. As shown in Table 2, RRLC and RRLE form abnormal higher and lower content of $\beta$-sheet, respectively, in the complex at the intermediate pH value (6.0). $\beta$-Sheet introduces inter-chain attraction by hydrogen bonding, which results in a heavy complexation process. As the pH jumps from 8.0 to 4.0, the formation of the extra $\beta$-sheet structure is triggered for RRLC. Because the formed secondary structure is difficult to dissociate, RRLC exhibits the strongest complexation behavior with ss-oligo, and the relaxation rate is also low compared with the other peptides (Fig. 1). RRLE shows an opposite trend. The $\beta$-sheet content reduces during the pH jump, which significantly deteriorates the complexation with ss-oligo.

## CONCLUSIONS

A series of pH-responsive peptides with the sequence of $(XXLY)_6SSSGSS$ are designed, and their complexation and coacervation processes with ss-oligo are studied by LLS and microscopy. The electrostatic interaction, whose strength is described by charge density or effective charges for a given length,

is the prerequisite for the formation of complexes or coacervates. The charge density also affects the relaxation of the polyelectrolytes in the coacervates. For our peptides containing 30 residues, 6 positive charges are safe for the complex formation with ss-oligo, while 9 charges to 12 charges are optimal considering both complexation and relaxation, generating coacervates with sizes even larger than those formed by peptides with higher charges. The effect of hydrophobicity is prominent when the charges are neutralized, which accounts at least partially for the growth of coacervates and the formation of solid precipitates. The secondary structures of peptides exhibit profound effect and the effect is even stronger than electrostatic interaction. Using *α*-helix as an example, the helical structure enhances both the chain rigidity and charge density, both of which can regulate the complexation and the phase separation processes, not to mention the exposure of specific residue groups. Therefore, the phase separation involving the secondary structure of peptides/proteins in most cases cannot be explained purely by electrostatic interactions. Moreover, the formation of secondary structures upon complexation, which is related to time and local concentration, makes the phase separation more "path dependent". A typical example is the solid-to-liquid transition with time. Our study gains insight into the phase separation process containing biopolymers, such as the formation of membraneless organelles, and helps fabricate coacervates with desirable structures and functions by *de novo* design and development.

## Conflict of Interests

The authors declare no interest conflict.

## Electronic Supplementary Information

Electronic supplementary information (ESI) is available free of charge in the online version of this article at http://doi.org/10.1007/s10118-024-3096-6.

## Data Availability Statement

The related data (DOI: 10.57760/sciencedb.j00189.00004) for this paper is available in the Data Repository of China Association for Science and Technology (https://www.scidb.cn/s/jAvlzq).

## ACKNOWLEDGMENTS

This work was financially supported by the National Natural Science Foundation of China (No. 21973002). The measurements of LCSM were performed at the Analytical Instrumentation Center of Peking University. We acknowledge the assistance and support from PKUAIC (Dr. Yan Guan).

## REFERENCES

1 Meka, V. S.; Singe, M. K. G.; Pichika, M. R.; Nali, S. R.; Kolapaili, V. R. M.; Kesharwani, P. A comprehensive review on polyelectrolyte complexes. *Drug Discov. Today* **2017**, *22*, 1697–1706.
2 Liu, H. D.; Sato, T. Polymer colloids formed by polyelectrolyte complexation of vinyl polymers and polysaccharides in aqueous solution. *Chinese J. Polym. Sci.* **2013**, *31*, 39–49.
3 Shi, X. H.; Chen, L.; Liu, B. W.; Long, J. W.; Xu, Y. J.; Wang, Y. Z. Carbon fibers decorated by polyelectrolyte complexes toward their epoxy resin composites with high fire safety. *Chinese J. Polym. Sci.* **2018**, *36*, 1375–1384.
4 Huang, W. T.; Li, J. F.; Liu, D. Z.; Tan, S. X.; Zhang, P. F.; Zhu, L. P.; Yang, S. G. Polyelectrolyte complex fiber of alginate and poly(diallyldimethylammonium chloride): humidity-induced shape memory and mechanical transition. *ACS Appl. Polym. Mater.* **2020**, *2*, 2119–2125.
5 Huang, W. T.; Liu, D. Z.; Zhu, L. P.; Yang, S. G. A salt controlled scalable approach for formation of polyelectrolyte complex fiber. *Chinese J. Chem.* **2020**, *38*, 465–470.
6 Yewdall, N. A.; André, A. A. M.; Lu, T. M.; Spruijt, E. Coacervates as models of membraneless organelles. *Curr. Opin. Colloid In.* **2021**, *52*, 101416.
7 Gao, N.; Mann, S. Membranized coacervate microdroplets: from versatile protocell models to cytomimetic materials. *Acc. Chem. Res.* **2023**, *56*, 297–307.
8 Mu, W. J.; Ji, Z.; Zhou, M. S.; Wu, J. Z.; Lin, Y. Y.; Qiao, Y. Membrane-confined liquid-liquid phase separation toward artificial organelles. *Sci. Adv.* **2021**, *7*, eabf9000.
9 Moreau, N. G.; Martin, N.; Gobbo, P.; Tang, T. Y. D.; Mann, S. Spontaneous membrane-less multi-compartmentalization via aqueous two-phase separation in complex coacervate microdroplets. *Chem. Commun.* **2020**, *56*, 12717–12720.
10 Blocher, W. C.; Perry, S. L. Complex coacervate-based materials for biomedicine. *Wires Nanomed Nanobi.* **2017**, *9*, e1442.
11 McTigue, W. C. B.; Perry, S. L. Protein encapsulation using complex coacervates: what nature has to teach us. *Small* **2020**, *16*, 1907671.
12 Sun, Y.; Lau, S. Y.; Lim, Z. W.; Chang, S. C.; Ghadessy, F.; Partridge, A.; Miserez, A. Phase-separating peptides for direct cytosolic delivery and redox-activated release of macromolecular therapeutics. *Nat. Chem.* **2022**, *14*, 274–283.
13 Ban, E.; Kim, A. Coacervates: recent developments as nanostructure delivery platforms for therapeutic biomolecules. *Int. J. Pharmaceut.* **2022**, *624*, 122058.
14 Johnson, N. R.; Wang, Y. D. Coacervate delivery systems for proteins and small molecule drugs. *Expert Opin. Drug. Del.* **2014**, *11*, 1829–1832.
15 Wang, J.; Abbas, M.; Huang, Y.; Wang, J.; Li, Y. Redox-responsive peptide-based complex coacervates as delivery vehicles with controlled release of proteinous drugs. *Commun. Chem.* **2023**, *6*, 243.
16 Turgeon, S. L.; Schmitt, C.; Sanchez, C. Protein-polysaccharide complexes and coacervates. *Curr. Opin. Colloid. In.* **2007**, *12*, 166–178.
17 Chen, S. J.; Guo, Q.; Yu, J. Bio-inspired functional coacervates. *Aggregate* **2022**, *3*, e293.
18 Stewart, R. J.; Wang, C. S.; Shao, H. Complex coacervates as a foundation for synthetic underwater adhesives. *Adv. Colloid Interface* **2011**, *167*, 85–93.
19 Forooshani, P. K.; Lee, B. P. Recent approaches in designing bioadhesive materials inspired by mussel adhesive protein. *J. Polym. Sci., Part A: Polym. Chem.* **2017**, *55*, 9–33.
20 Rumyantsev, A. M.; Jackson, N. E.; de Pablo, J. J. Polyelectrolyte complex coacervates: recent developments and new frontiers. *Annu. Rev. Conden. Ma. P* **2021**, *12*, 155–176.
21 Oparin, A. I. *The Origin of Life*. MacMillan: New York, **1938**, 1–6.
22 Fry, I. The origins of research into the origins of life. *Endeavour* **2006**, *30*, 24–28.
23 Gözen, I.; Köksal, E. S.; Poldsalu, I.; Xue, L.; Spustova, K.; Pedrueza-

Villalmanzo, E.; Ryskulov, R.; Meng, F. D.; Jesorka, A. Protocells: milestones and recent advances. *Small* **2022**, *18*, 2106624.
24 Li, F.; Lin, Y. Y.; Qiao, Y. Regulating FUS liquid-liquid phase separation *via* specific metal recognition. *Chinese J. Polym. Sci.* **2022**, *40*, 1043−1049.
25 Veis, A. A review of the early development of the thermodynamics of the complex coacervation phase separation. *Adv. Colloid Interface* **2011**, *167*, 2−11.
26 Sing, C. E.; Perry, S. L. Recent progress in the science of complex coacervation. *Soft Matter* **2020**, *16*, 2885−2914.
27 Overbeek, J. T. G. a. V., M. J. Phase separation in polyelectrolyte solutions. Theory of complex coacervation. *J. Cell. Comp. Physiol.* **1957**, *49*, 7−26.
28 Michaeli, I.; Overbeek, J. T. G.; Voorn, M. J. Phase separation of polyelectrolyte solutions. *J. Polym. Sci.* **1957**, *23*, 443−450.
29 Shi, A. C.; Noolandi, J. Theory of inhomogeneous weakly charged polyelectrolytes. *Macromol. Theor. Simul.* **1999**, *8*, 214−229.
30 Wang, Q.; Taniguchi, T.; Fredrickson, G. H. Self-consistent field theory of polyelectrolyte systems. *J. Phys. Chem. B* **2004**, *108*, 6733−6744.
31 Shusharina, N. P.; Zhulina, E. B.; Dobrynin, A. V.; Rubinstein, M. Scaling theory of diblock polyampholyte solutions. *Macromolecules* **2005**, *38*, 8870−8881.
32 Wang, Z. W.; Rubinstein, M. Regimes of conformational transitions of a diblock polyampholyte. *Macromolecules* **2006**, *39*, 5897−5912.
33 Sing, C. E. Development of the modern theory of polymeric complex coacervation. *Adv. Colloid Interface* **2017**, *239*, 2−16.
34 Tabandeh, S.; Leon, L. Engineering peptide-based polyelectrolyte complexes with increased hydrophobicity. *Molecules* **2019**, *24*, 868.
35 Huang, J.; Laaser, J. E. Charge density and hydrophobicity-dominated regimes in the phase behavior of complex coacervates. *ACS Macro Lett.* **2021**, *10*, 1029−1034.
36 Vieregg, J. R.; Lueckheide, M.; Marciel, A. B.; Leon, L.; Bologna, A. J.; Rivera, J. R.; Tirrell, M. V. Oligonucleotide-peptide complexes: phase control by hybridization. *J. Am. Chem. Soc.* **2018**, *140*, 1632−1638.
37 Pacalin, N. M.; Leon, L.; Tirrell, M. Directing the phase behavior of polyelectrolyte complexes using chiral patterned peptides. *Eur. Phys. J.-Spec. Top.* **2016**, *225*, 1805−1815.
38 Cheng, C.; Tu, Z. C.; Wang, H. pH-induced complex coacervation of fish gelatin and carboxylated chitosan: phase behavior and structural properties. *Food Res. Int*. **2023,** *167*, 112652.
39 Kaibara, K.; Okazaki, T.; Bohidar, H. B.; Dubin, P. L. pH-induced coacervation in complexes of bovine serum albumin and cationic polyelectrolytes. *Biomacromolecules* **2000**, *1*, 100−107.
40 Priftis, D.; Tirrell, M. Phase behaviour and complex coacervation of aqueous polypeptide solutions. *Soft Matter* **2012**, *8*, 9396−9405.
41 Perry, S. L.; Li, Y.; Priftis, D.; Leon, L.; Tirrell, M. The effect of salt on the complex coacervation of vinyl polyelectrolytes. *Polymers* **2014**, *6*, 1756−1772.
42 Love, C.; Steinkühler, J.; Gonzales, D. T.; Yandrapalli, N.; Robinson, T.; Dimova, R.; Tang, T. Y. D. Reversible pH-responsive coacervate formation in lipid vesicles activates dormant enzymatic reactions. *Angew. Chem. Int. Ed.* **2020**, *59*, 5950−5957.
43 Zhou, J.; Wan, Y.; Cohen Stuart, M. A.; Wang, M.; Wang, J. Effects of control factors on protein-polyelectrolyte complex coacervation. *Biomacromolecules* **Article ASAP**.
44 Mart, R. J.; Osborne, R. D.; Stevens, M. M.; Ulijn, R. V. Peptide-based stimuli-responsive biomaterials. *Soft Matter* **2006**, *2*, 822−835.
45 Ulijn, R. V.; Woolfson, D. N. Peptide and protein based materials in 2010: from design and structure to function and application. *Chem Soc Rev* **2010**, *39*, 3349−3350.
46 Wang, L.; Wang, N. X.; Zhang, W. P.; Cheng, X. R.; Yan, Z. B.; Shao, G.; Wang, X.; Wang, R.; Fu, C. Y. Therapeutic peptides: current applications and future directions. *Signal Transduct Tar.* **2022**, *7*, 48.
47 Bai, Q. W.; Zhang, Q. F.; Jing, H. R.; Chen, J. X.; Liang, D. H. Liquid-Liquid Phase Separation of Peptide/Oligonucleotide Complexes in Crowded Macromolecular Media. *J. Phys. Chem. B* **2021**, *125*, 49−57.
48 Kyte, J.; Doolittle, R. F. A simple method for displaying the hydropathic character of a protein. *J. Mol. Biol.* **1982**, *157*, 105−132.
49 Stothard, P. The sequence manipulation suite: JavaScript programs for analyzing and formatting protein and DNA sequences. *Biotechniques* **2000**, *28*, 1102−1104.
50 Lehninger, A. L.; Nelson, D. L.; Cox, M. M. *Principles of Biochemistry*. Worth Publishers: New York, **1982**, 615−643.
51 Wang, H.; Davis, R. H. Collective effects of gravitational and Brownian coalescence on droplet growth. *J Colloid Interf. Sci.* **1996**, *178*, 47−52.

https://doi.org/10.1007/s10118-024-3096-6